Ruthenium–Carbene Functionality Bonded to Dibenzotetramethyltetraaza[14]annulene: Metal-to-Macrocycle Ligand-Induced Carbene Migration

Alain Klose, Euro Solari, Joëlle Hesschenbrouck, and Carlo Floriani*

Institut de Chimie Minérale et Analytique, BCH, Université de Lausanne, CH-1015 Lausanne, Switzerland

Nazzareno Re

Facoltà di Farmacia, Università degli Studi "G. D'Annunzio", I-66013 Chieti, Italy

Silvano Geremia and Lucio Randaccio

Dipartimento di Scienze Chimiche, Università di Trieste, I-34127 Trieste, Italy

This report contains the chemistry of the ruthenium–carbene functionality bonded to the dibenzotetramethyltetraaza[14]annulene dianion, tmtaa. [{Ru(tmtaa)}$_2$(μ-C$_8$H$_{12}$)], **1**, was the most appropriate starting material, as it contains a labile olefin, which can be displaced by a number of ligands to give [Ru(tmtaa)(L)(L′)] [L = L′ = Py, **2**; L = CO, L′ = thf, **3**; L = Bu^{t}NC, L′ = thf, **4**; L = L′ = Bu^{t}NC, **5**]. Reaction of **1** with diazoalkanes led to the displacement of the olefin and gave the corresponding carbene derivatives [Ru(tmtaa)(CRR′)] [R = R′ = Ph, **6**; R = Ph, R′ = H, **7**; R = Ph, R′ = COOMe, **8**], which have square-pyramidal structures. Complexes **7** and **8** underwent a remarkable labilization of the carbene functionality in the reaction with carbon monoxide, while **6** was only converted to the corresponding carbonyl [Ru(tmtaa)(CPh$_2$)(CO)], **10**, by CO. The reaction of **7** with both CO and Bu^{t}NC led to the migration of the carbene to one of the metalladiimino rings of the ligands in **12** and **13**, while the reaction of **8** with both CO and Bu^{t}NC enabled us to intercept the preliminary product of a free-radical-type migration of the carbene to the tmtaa ligand, with the isolation of **11** and **14**. The ligand (CO or Bu^{t}NC)-induced migration of the CR$_2$ fragment to the macrocycle seemed to proceed via a carbene mechanism in the case of **7**, while **8** seemed to prefer a free-radical-like pathway. This assumption was further supported by extended Hückel calculations and by the reaction of **6**–**8** with ligands of different σ/π donor/acceptor capability. The pyridine converted **6**–**8** to the corresponding coordinate adducts, **15**–**17**, while the reaction of **7** with PMe$_3$ led to the formation of [Ru(tmtaa)(PMe$_3$)$_2$] and stilbenes, via a plausible carbene mechanism. The reaction of **8** with PMe$_3$ proceeded through a free-radical pathway leading to **19**, which has a structure similar to **11** and **14**. The ligand-induced labilization of the metallacarbene functionality in the macrocyclic environment was analyzed using the extended Hückel calculations.

Introduction

The use of macrocycles as ancillary ligands, which until recently has been confined to coordination chemistry, is now becoming more and more popular in organometallic chemistry.[1] The results so far obtained have led to the recognition of a "macrocyclic effect" similar to that found in coordination chemistry, though with a different meaning. Two important directions have been taken in the field: the first one involves the use of early transition metals, and the second one considers the effect of specific macrocycles. The ancillary ligand can, of course, have a pronounced effect on the outcome of the chemistry, with a number of ligands being targeted because of their interesting electronic and steric properties. One such ligand is dibenzotetra-

methyltetraaza[14]annulene dianion, abbreviated as tmtaa (Chart 1).[2]

The tmtaa ligand has a number of major characteristics which make its effect particularly suitable to study. First, the geometry of the ligand is directly related to the d^n configuration of the complexed metal and can assume either an almost square-planar or a very pronounced saddle shape conformation.[2d] In the first case, the two available reactive sites are usually trans, whereas in the latter they have a cis relationship. Contrary to the porphyrins and analogously to what is found in Schiff-base chemistry, another peculiarity of the tmtaa ligand lies in the possibility of the ligand undergoing chemical modifications when studying the metal reactivity. Our initial work in the area of Ru–macrocyclic chemistry took advantage of this ligand. The first synthesis of a Ru–tmtaa complex was reported by

Chart 1
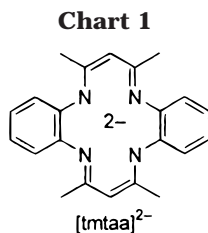
[tmtaa]$^{2-}$

Goedken, in a preliminary form and described [Ru-(tmtaa)]$_2$.[3] The isolation of well-defined monomeric forms was later reported by Cotton, who prepared [Ru-(tmtaa)(PMePh$_2$)$_2$],[4] and subsequently the similar [Ru-(Me$_4$tmtaa)(PPh$_3$)$_2$] complex was reported.[5] The [Ru-(tmtaa)] fragment can provide a particularly useful entry into the organometallic chemistry of ruthenium, by stressing the differences in the chemical behavior of the metal depending on the nature of the macrocyclic ligand. As a matter of fact, the organometallic chemistry of the Ru−macrocycle has been confined so far almost exclusively to porphyrin ligands.[6] We report here the synthesis of a starting material that can be considered as a particularly suitable source of the [Ru(tmtaa)] fragment along with the synthesis of the [Ru(tmtaa)-

CR$_2$] carbene complexes, whose reactivity involves both the metal and the ancillary ligand tmtaa. Within this context a particularly interesting aspect of the [Ru=CR$_2$] chemistry is the ligand-induced carbene labilization. This kind of labilization can be related to the catalytic activity of ruthenium−carbenes inducing metathesis reactions.[7] Extended Hückel calculations enabled us to correlate the structure and electronic properties of the Ru−carbene functionality in the two completely different environments and its labilization induced by a ligand as having an appropriate balance between σ-donating and π-accepting properties. A preliminary account of the reaction of [Ru(tmtaa)CR$_2$] with CO has been communicated.[8]

Experimental Section

General Procedure. All reactions were carried out under an atmosphere of purified nitrogen. Solvents were dried and distilled before use by standard methods. ^{1}H NMR and IR spectra were recorded on AC-200, DPX-400 Bruker, and Perkin-Elmer FT 1600 instruments, respectively. The syntheses of [Ru(COD)Cl$_2$]$_2$,[9] tmtaaH$_2$,[2d] Ph$_2$CN$_2$,[10] PhHCN$_2$,[11] Ph-(COOMe)CN$_2$,[12] have been carried out according to the literature.

Synthesis of 1. To a THF solution (550 mL) of tmtaaH$_2$ (13.7 g, 39.7 mmol) was added dropwise a solution of Bu^{t}Li in *n*-hexane (1.64 M, 80.0 mmol). After stirring for 3 h, degassed [(COD)RuCl$_2$] (11.1 g, 39.7 mmol) was added, and the red solution stirred for a further 20 h. The resulting brown microcrystalline product was filtered, washed with THF (30 mL), and dried in vacuo (17.5 g, 82%). Potentiometric analysis showed that the product did not contain any chloride ion. Anal. Calcd for [{Ru(tmtaa)}$_2$(μ-C$_8$H$_{12}$)]·thf, C$_{56}$H$_{64}$N$_8$ORu$_2$: C, 63.48; H, 6.04; N, 10.56. Found: C, 63.10; H, 6.44; N, 9.58. ^{1}H NMR (C$_5$D$_5$N, 200 MHz, 298 K, ppm): δ 6.77−6.72 (m, 4H, Ar); 6.32−6.27 (m, 4H, Ar); 5.56 (s, 2H, COD−CH); 4.04 (s, 2H, CH); 3.64 (m, 2H, THF); 2.25 (s, 4H, COD−CH$_2$); 1.95 (s, 12H, CH$_3$); 1.59 (m, 2H, THF).

Synthesis of 2. To a toluene suspension (100 mL) of 1·thf (0.93 g, 0.87 mmol) was added pyridine (0.35 mL, 4.35 mL). The mixture was stirred overnight to give a red solution, which was then filtered. Solvent was removed in vacuo to 15 mL and *n*-hexane (30 mL) added. The red product was filtered, washed with *n*-hexane (30 mL), and dried in vacuo (0.75 g, 72%). Anal. Calcd for [Ru(tmtaa)(Py)$_2$]·C$_7$H$_8$, C$_{39}$H$_{40}$N$_6$Ru: C, 67.51; H, 5.81; N, 12.11. Found: C, 66.95; H, 6.03; N, 12.17. ^{1}H NMR (C$_6$D$_6$, 200 MHz, 298 K, ppm): δ 9.58 (s, 4H, py); 7.09−6.24 (m, 19H, Ar); 4.01 (s, 2H, CH); 2.10 (s, 3H, toluene); 1.89 (s, 12H, CH$_3$).

Synthesis of 3. A brown THF suspension (150 mL) of 1·thf (2.1 g, 1.97 mmol) was cooled (−20 °C) and then saturated with CO to give a solution which was kept under CO overnight and then concentrated to 10 mL. *n*-Hexane (20 mL) was added, and the crystalline product filtered and dried in vacuo (1.36

(1) For some general references see: Collman, J. P.; Hegedus, L. S.; Norton, J. R.; Finke, R. G. *Principles and Applications of Organotransition Metal Chemistry*; University Science Books: Mill Valley, CA, 1987. For porphyrins, see: Brand, H.; Arnold, J. *Angew. Chem., Int. Ed. Engl.* **1994**, *33*, 95. Brand, H.; Arnold, J. *Organometallics* **1993**, *12*, 3655. Kim, H.-J.; Whang, D.; Kim K.; Do, Y. *Inorg. Chem.* **1993**, *32*, 360. Arnold, J.; Johnson, S. E.; Knobler, C. B.; Hawthorne, M. F. *J. Am. Chem. Soc.* **1992**, *114*, 3996. Brand H.; Arnold, J. *J. Am. Chem. Soc.* **1992**, *114*, 2266. Brand, H.; Arnold, J. *Coord. Chem. Rev.* **1995**, *140*, 137. Aida, T.; Inoue, S. *Acc. Chem. Res.* **1996**, *29*, 39, and ref 6. For *meso*-octaalkylporphyrinogen, see: Jacoby, D.; Floriani, C.; Chiesi-Villa, A.; Rizzoli, C. *J. Chem. Soc., Chem. Commun.* **1991**, 790. Jacoby, D.; Floriani, C.; Chiesi-Villa, A.; Rizzoli, C. *J. Am. Chem. Soc.* **1993**, *115*, 3595. Jacoby, D.; Floriani, C.; Chiesi-Villa, A.; Rizzoli, C. *J. Am. Chem. Soc.* **1993**, *115*, 7025. Rosa, A.; Ricciardi, G.; Rosi, M.; Sgamellotti, A.; Floriani, C. *J. Chem. Soc., Dalton Trans.* **1993**, 3759. Solari, E.; Musso, F.; Floriani, C.; Chiesi-Villa, A.; Rizzoli, C. *J. Chem. Soc., Dalton Trans.* **1994**, 2015. Jacoby, D.; Isoz, S.; Floriani, C.; Chiesi-Villa, A.; Rizzoli, C. *J. Am. Chem. Soc.* **1995**, *117*, 2793. Jacoby, D.; Isoz, S.; Floriani, C.; Chiesi-Villa, A.; Rizzoli, C. *J. Am. Chem. Soc.* **1995**, *117*, 2085. For calix[4]arenes, see: Giannini, L.; Solari, E.; Zanotti-Gerosa, A.; Floriani, C.; Chiesi-Villa, A.; Rizzoli, C. *Angew. Chem., Int. Ed. Engl.* **1996**, *35*, 85 and 2825; **1997**, *36*, 753. Castellano, B.; Zanotti-Gerosa, A.; Solari, E.; Floriani, C.; Chiesi-Villa, A.; Rizzoli, C. *Organometallics* **1996**, *15*, 4894. Giannini, L.; Caselli, A.; Solari, E.; Floriani, C.; Chiesi-Villa, A.; Rizzoli, C.; Re, N.; Sgamellotti, A. *J. Am. Chem. Soc.* **1997**, *119*, 9198 and 9709. Caselli, A.; Giannini, L.; Solari, E.; Floriani, C.; Chiesi-Villa, A.; Rizzoli, C. *Organometallics* **1997**, *16*, 5457. Zanotti-Gerosa, A.; Solari, E.; Giannini, L.; Floriani, C.; Chiesi-Villa, A.; Rizzoli, C. *J. Am. Chem. Soc.* **1998**, *120*, 437. Giannini, L.; Solari, E.; Floriani, C.; Chiesi-Villa, A.; Rizzoli, C. *J. Am. Chem. Soc.* **1998**, *120*, 823.

(2) Some leading references in the use of [tmtaa]$^{2-}$ as ancillary ligand in the organometallic chemistry of the early transition metals are: (a) Goedken, V. L.; Ladd, J. A. *J. Chem. Soc., Chem. Commun.* **1981**, 910; **1982**, 142. (b) Floriani, C.; Ciurli, S.; Chiesi-Villa, A.; Guastini, C. *Angew. Chem., Int. Ed. Engl.* **1987**, *26*, 70. (c) Solari, E.; De Angelis, S.; Floriani, C.; Chiesi-Villa, A.; Rizzoli, C. *Inorg. Chem.* **1992**, *31*, 96. (d) De Angelis, S.; Solari, E.; Gallo, E.; Floriani, C.; Chiesi-Villa, A.; Rizzoli, C. *Inorg. Chem.* **1992**, *31*, 2520. (e) Giannini, L.; Solari, E.; Floriani, C.; Chiesi-Villa, A.; Rizzoli, C. *Angew. Chem., Int. Ed. Engl.* **1994**, *33*, 2204. (f) Giannini, L.; Solari, E.; De Angelis, S.; Ward, T. R.; Floriani, C.; Chiesi-Villa, A.; Rizzoli, C. *J. Am. Chem. Soc.* **1995**, *117*, 5801. (g) Black, D. G.; Swenson, D. C.; Jordan, R. F. *Organometallics* **1995**, *14*, 3539. (h) Blake, A. J.; Mountford, P.; Nikonov, G. I.; Swallow, D. *Chem. Commun.* **1996**, 1835. (i) Schumann, H. *Inorg. Chem.* **1996**, *35*, 1808. (j) Nikonov, G. I.; Blake, A. J.; Mountford, P. *Inorg. Chem.* **1997**, *36*, 1107. Black, D. G.; Jordan, R. F.; Rogers, R. D. *Inorg. Chem.* **1997**, *36*, 103. Martin, A.; Uhrhammer, R.; Gardner, T. G.; Jordan, R. F. *Organometallics* **1998**, *17*, 382. Mountford, P. *Chem. Soc. Rev.* **1998**, *27*, 105.

(3) Warren, L. F.; Goedken, V. L. *J. Chem. Soc., Chem. Commun.* **1978**, 909.

(4) Cotton, F. A.; Czuchajowska, J. *Polyhedron* **1990**, *9*, 1221.

(5) Luo, L.; Stevens, E. D.; Nolan, S. P. *Inorg. Chem.* **1996**, *35*, 252.

(6) Collman, J. P.; Barnes, C. E.; Swepston, P. N.; Ibers, J. A. *J. Am. Chem. Soc.* **1984**, *106*, 3500. Collman, J. P.; Brothers, P. J.; Mc-Elwee-White, L.; Rose, E.; Wright, L. J. *J. Am. Chem. Soc.* **1985**, *107*, 4570. Collman, J. P.; Brothers, P. J.; Mc-Elwee-White, L.; Rose, E. *J. Am. Chem. Soc.* **1985**, *107*, 6110.

(7) (a) Grubbs, R. H.; Miller, S. J.; Fu, G. C. *Acc. Chem. Res.* **1995**, *28*, 446. (b) Nguyen, S. T.; Grubbs, R. H.; Ziller, J. W. *J. Am. Chem. Soc.* **1993**, *115*, 9858. (c) Miller, S. J.; Blackwell, H. E.; Grubbs, R. H. *J. Am. Chem. Soc.* **1996**, *118*, 9606. (d) Mohr, B.; Linn, D. M.; Grubbs, R. H. *Organometallics* **1996**, *15*, 4317.

(8) Klose, A.; Solari, E.; Floriani, C.; Geremia, S.; Randaccio, L. *Angew. Chem., Int. Ed. Engl.* **1998**, *37*, 148.

(9) Powell, J.; Shaw, B. L. *J. Chem. Soc. (A)* **1968**, 159.

(10) Smith, L. I.; Howard, K. L. *Organic Syntheses*; Wiley: New York, 1955; Vol. 3, p 351.

(11) Yates, P.; Shapiro, L. *J. Org. Chem.* **1958**, *23*, 759.

(12) Ciganek, E. J. *J. Org. Chem.* **1970**, *35*, 862.

g, 63%). Anal. Calcd for [Ru(tmtaa)(CO)(thf)], $C_{27}H_{30}N_4O_2Ru$: C, 59.65; H, 5.56; N, 10.31. Found: C, 59.58; H, 5.34; N, 10.27. ^{1}H NMR (C_6D_6, 200 MHz, 298 K, ppm): δ 6.75–6.70 (m, 4H, Ar); 6.54–6.49 (m, 4H, Ar); 4.43 (s, 2H, CH); 3.58 (m, 4H, THF); 1.96 (s, 12H, CH_3); 1.33 (m, 4H, THF). ^{13}C NMR (C_6D_6, 50.3 MHz, 298 K, ppm): δ 217.4 (CO), 156.4, 149.6, 122.1, 121.4, 68.2, 25.2, 24.9.

Synthesis of 4. To a brown THF suspension (100 mL) of **1**·thf (1.44 g, 1.34 mmol) was added dropwise a THF solution (30 mL) of Bu^{t}NC (0.24 g, 2.8 mmol). The color slowly became dark green, and a new microcrystalline product precipitated. The reaction was stirred overnight and then concentrated to 30 mL. n-Hexane (15 mL) was added, and the product filtered and dried in vacuo (0.82 g, 51%). Anal. Calcd for [Ru(tmtaa)-(Bu^{t}NC)(thf)], $C_{31}H_{39}N_5ORu$: C, 62.19; H, 6.57; N, 11.70. Found: C, 62.03; H, 6.70; N, 11.93. ^{1}H NMR (C_5D_5N, 200 MHz, 298 K, ppm): δ 6.84–6.79 (m, 4H, Ar); 6.55–6.52 (m, 4H, Ar); 4.00 (s, 2H, CH); 3.63 (m, 4H, THF); 1.89 (s, 12H, CH_3); 1.59 (m, 4H, THF); 1.23 (s, 9H, Bu^t). ^{13}C NMR (C_5D_5N, 50.3 MHz, 298 K, ppm): δ 194.0 (CN), 153.9, 151.5, 121.5, 120.9, 111.7, 67.8, 32.5, 25.8, 24.7.

Synthesis of 5. To a THF suspension (120 mL) of **1**·thf (1.99 g, 1.87 mmol) was added dropwise a THF solution (50 mL) of Bu^{t}NC (0.66 g, 8.0 mmol). Complete solubilization was observed, and the solution stirred overnight. The volume was decreased in vacuo to 10 mL, and n-hexane (25 mL) added. The crystalline product was filtered, then washed with n-hexane (20 mL) and dried in vacuo (1.35 g, 59%). Anal. Calcd for [Ru(tmtaa)(Bu^{t}NC)$_2$], $C_{32}H_{40}N_6Ru$: C, 63.03; H, 6.61; N, 13.78. Found: C, 63.10; H, 6.75; N, 13.53. ^{1}H NMR (C_6D_6, 200 MHz, 298 K, ppm): δ 6.67–6.63 (m, 4H, Ar); 6.39–6.34 (m, 4H, Ar); 4.22 (s, 2H, CH); 1.88 (s, 12H, CH_3); 1.11 (s, 18H, Bu^t). ^{13}C NMR (C_6D_6, 50.3 MHz, 298 K, ppm): δ 164.7 (CN). Crystals for X-ray analysis were obtained from toluene and analyzed as solvated forms.

Synthesis of 6. To a THF suspension (150 mL) of **1**·thf (3.77 g, 3.53 mmol) was added a THF solution (50 mL) of diphenyl-diazomethane (1.38 g, 7.10 mmol). The mixture slowly became soluble with the concomitant evolution of nitrogen gas. The solution was stirred for 36 h and then concentrated to 10 mL. n-Hexane was added (30 mL), and the microcrystalline material filtered and dried in vacuo (3.55 g, 74%). Crystals suitable for X-ray analysis were grown in THF/n-hexane. Anal. Calcd for [Ru(tmtaa)(CPh$_2$)]·thf, $C_{39}H_{40}N_4ORu$: C, 68.70; H, 5.91; N, 8.22. Found: C, 68.78; H, 5.99; N, 8.52. ^{1}H NMR (C_6D_6, 200 MHz, 298 K, ppm): δ 6.92–6.88 (m, 4H, Ar); 6.73–6.69 (m, 4H, Ar); 6.45 (m, 10H, Ph); 4.91 (s, 2H, CH); 3.56 (m, 4H, THF); 2.13 (s, 12H, CH_3); 1.40 (m, 4H, THF). ^{13}C NMR (C_6D_6, 50.3 MHz, 298 K, ppm): δ 291.8 (C carbene). THF was kept even when the solid was dried in vacuo for a long time.

Synthesis of 7. To a cooled (-30 °C) THF suspension (150 mL) of **1**·thf (2.09 g, 1.96 mmol) was added phenyldiaz-omethane (0.47 g, 3.92 mmol). The reaction occurred immediately with the concomitant evolution of nitrogen gas. The solution was allowed to warm to room temperature and stirred overnight. Solvent was removed to 10 mL, and n-hexane (25 mL) added. The crystalline product was filtered and dried in vacuo (1.34 g, 64%). Anal. Calcd for [Ru(tmtaa)(CHPh)], $C_{29}H_{28}N_4Ru$: C, 65.27; H, 5.29; N, 10.50. Found: C, 64.83; H, 5.34; N, 10.28. ^{1}H NMR (CD_2Cl_2, 400 MHz, 298 K, ppm): δ 17.1 (s, 1H, CH carbene); 7.22–6.79 (m, 13H, Ar); 4.90 (s, 2H, CH); 2.44 (s, 12H, CH_3). ^{13}C NMR (CD_2Cl_2, 100.6 MHz, 298 K, ppm): δ 156.1, 154.9, 150.2, 128.9, 126.9, 125.9, 122.6, 122.0, 109.4, 25.4.

Synthesis of 8. To a cooled (-20 °C) THF suspension (150 mL) of **1**·thf (1.65 g, 1.54 mmol) was added diazomethylphe-nylglyoxylate (0.60 g, 3.40 mmol). The suspension was allowed to warm to room temperature and stirred overnight. The mixture slowly became soluble with the concomitant evolution of nitrogen gas. The solution was filtered and the solvent reduced to 15 mL. n-Hexane (20 mL) was added dropwise, and

the resulting microcrystalline product filtered and dried in vacuo (1.09 g, 60%). Anal. Calcd for [Ru(tmtaa){C(Ph)-(COOMe)}], $C_{31}H_{30}N_4O_2Ru$: C, 62.93; H, 5.11; N, 9.47. Found: C, 62.68; H, 5.17; N, 9.63. ^{1}H NMR (C_6D_6, 200 MHz, 298 K, ppm): δ 6.91–6.83 (m, 9H, Ar); 6.64–6.60 (m, 4H, Ar); 4.91 (s, 2H, CH); 3.04 (s, 3H, CH_3 COO); 2.20 (s, 12H). ^{13}C NMR (C_6D_6, 100.6 MHz, 298 K, ppm): δ 279.2 (C carbene), 178.3, 156.1, 153.5, 149.7, 127.2, 126.1, 122.1, 121.8, 120.9, 110.8, 50.4, 25.4.

Synthesis of 9. To a cooled (-40 °C) brown THF suspension (140 mL) of **1**·thf (1.92 g, 1.79 mmol) was added via seringe (o-Me$_3$Si)PhNC (0.69 g, 3.59 mmol). A sudden color change to dark red was observed. The suspension was allowed to warm to room temperature and stirred overnight to give a solution. The solvent was removed to 5 mL, and n-hexane (40 mL) added. The crystalline solid was filtered and dried in vacuo (1.88 g, 84%). The solid did not lose THF in vacuo. Anal. Calcd for [Ru(tmtaa)(o-Me$_3$SiOC$_6$H$_4$NC)]·thf, $C_{36}H_{43}N_5O_2SiRu$: C, 61.17; H, 6.13; N, 9.91. Found: C, 60.99; H, 6.09; N, 9.87. ^{1}H NMR (C_6D_6, 200 MHz, 298 K, ppm): δ 6.95–6.53 (m, 12H, Ar); 4.47 (s, 2H, CH); 3.66 (m, 4H, THF); 2.02 (s, 12H, CH_3); 1.40 (m, 4H, THF); 0.21 (s, 9H, Me$_3$). ^{13}C NMR (C_6D_6, 100.6 MHz, 298 K, ppm): δ 208.8 (CN), 155.4, 150.5, 129.6, 125.2, 122.3, 121.7, 121.6, 121.1, 110.7, 68.1, 25.5, 24.8.

Synthesis of 10. A THF suspension (100 mL) of **6**·thf (1.20 g, 1.76 mmol) was cooled to -30 °C and then saturated with CO. No change of color was observed. The suspension was allowed to warm to room temperature and stirred for 5 h to give a solution. Solvent was removed to dryness, and the product treated with n-hexane (20 mL). The resulting suspension was filtered, and the product dried in vacuo (0.68 g, 61%). Anal. Calcd for [Ru(tmtaa)(CPh$_2$)(CO)], $C_{36}H_{32}N_4ORu$: C, 67.80; H, 5.06; N, 8.78. Found: C, 67.90; H, 5.28; N, 9.20. IR (Nujol, ν_{max}/cm^{-1}): 1906 (m, CO). ^{1}H NMR (C_6D_6, 200 MHz, 298 K, ppm): δ 6.92–6.89 (m, 4H, Ar); 6.74–6.70 (m, 4H, Ar); 6.45 (m, 10H, Ph); 4.92 (s, 2H, CH); 2.13 (s, 12H, CH_3). ^{13}C NMR (C_6D_6, 100.6 MHz, 298 K, ppm): δ 291.7 (C carbene), 270.9 (CO).

Synthesis of 11. An orange THF solution (100 mL) of **8** (0.58 g, 0.98 mmol) was cooled (0 °C) and then saturated with CO. The solution immediately became red and was then kept overnight under CO. The solvent was removed in vacuo, the product was then treated with n-hexane (30 mL) and filtered, and the resulting solid was dried in vacuo (0.39 g, 64%). Anal. Calcd for **11**, $C_{32}H_{30}N_4O_3Ru$: C, 62.02; H, 4.88; N, 9.04. Found: C, 61.50; H, 5.10; N, 8.92. IR (Nujol, ν_{max}/cm^{-1}): 1905 (s, CO), 1732 (m, COO), 1628 (m). ^{1}H NMR (C_6D_6, 400 MHz, 298 K, ppm): δ 7.87–6.51 (m, 13H, Ar); 4.65 (s, 1H, HC=C); 4.48 (s, 1H, CH); 3.59 (s, 3H, OCH_3); 2.01 (s, 6H, CH_3); 1.88 (s, 6H, CH_3). ^{13}C NMR (C_6D_6, 100.6 MHz, 298 K, ppm): δ 211.9 (CO). Crystals suitable for X-ray analysis were grown in toluene/n-hexane (1/1) and contained toluene of crystallization.

Synthesis of 12. An orange toluene suspension (100 mL) of **7** (0.93 g, 1.74 mmol) was cooled (-35 °C) and then saturated with CO. The suspension turned green and slowly, on warming to room temperature, dissolved to give a red solution. After 2 h stirring, the solvent was removed to 10 mL, and n-hexane added (20 mL). The crystalline product was filtered and dried in vacuo (0.73 g, 71%). Anal. Calcd for **12**, $C_{31}H_{28}N_4O_2Ru$: C, 63.15; H, 4.79; N, 9.50. Found: C, 63.08; H, 4.53; N, 9.36. IR (Nujol, ν_{max}/cm^{-1}): 2016 (s, CO), 1948 (s, CO). ^{1}H NMR (C_6D_6, 400 MHz, 298 K, ppm): δ 7.44–6.61 (m, 13H, Ar); 5.20 (s, 1H, HC=C); 3.18 (d, J = 14.7 Hz, 1H, CH$_2$); 2.52 (s, 3H, CH_3); 2.48 (d, J = 14.7 Hz, 1H, CH$_2$); 2.29 (s, 3H, CH_3); 2.19 (s, 3H, CH_3); 1.39 (s, 3H, CH_3). ^{13}C NMR (C_6D_6, 100.6 MHz, 298 K, ppm): δ 199.8, 197.5. Crystals suitable for X-ray analysis were grown in toluene/n-hexane (1/1) and contained toluene of crystallization.

Synthesis of 13. To a cooled (-20 °C) stirred red toluene suspension (100 mL) of **7** (1.27 g, 2.39 mmol) was added a toluene solution (40 mL) of Bu^{t}NC (0.40 g, 4.78 mmol).

Warming to room temperature and stirring for 3 h gave a green solution. The solvent was removed to 5 mL, *n*-hexane (30 mL) was added, and the solution was left to stand for 1 h. The resulting green crystalline solid was collected by filtration and dried in vacuo (0.89 g, 54%). Anal. Calcd for **13**, $C_{39}H_{46}N_6$-Ru: C, 66.93; H, 6.62; N, 12.01. Found: C, 66.01; H, 6.52; N, 11.95. IR (Nujol, ν_{max}/cm^{-1}): 2095 (s, CN), 1595 (s), 1565 (s).^{1}H NMR (C_6D_6, 400 MHz, 298 K, ppm): δ 7.61–6.43 (m, 13H, Ar); 5.69 (d, J = 13.1 Hz, 1H, CH$_2$); 5.04 (s, 1H, HC=C); 3.43 (d, J = 13.1 Hz, 1H, CH$_2$); 2.56 (s, 3H, CH$_3$); 2.54 (s, 3H, CH$_3$); 2.45 (s, 3H, CH$_3$); 1.99 (s, 3H, CH$_3$); 0.96 (s, 9H, Bu^t); 0.82 (s, 9H, Bu^t). ^{13}C NMR (C_6D_6, 100.6 MHz, 298 K, ppm): δ 173.9, 160.4.

Synthesis of 14. To a cooled (−20 °C) red toluene suspension (100 mL) of **8** (1.04 g, 1.75 mmol) was added a toluene solution (30 mL) of Bu^{t}NC (0.15 g, 1.75 mmol). Warming to room temperature and stirring for 24 h gave a green solution. The solvent was removed to 10 mL, and *n*-hexane (20 mL) added. The microcrystalline solid was then filtered and dried in vacuo (0.74 g, 63%). Anal. Calcd for **14**, $C_{36}H_{39}N_5O_2$Ru: C, 64.08; H, 5.83; N, 10.38. Found: C, 64.97; H, 5.91; N, 9.32. IR (Nujol, ν_{max}/cm^{-1}): 1935 (s, CN), 1628 (s, COO).^{1}H NMR (C_6D_6, 400 MHz, 298 K, ppm): δ 7.93–6.49 (m, 13H, Ar); 4.70 (s, 1H, HC=C); 4.58 (s, 1H, CH); 3.69 (s, 3H, OCH$_3$); 2.09 (s, 6H, CH$_3$); 1.95 (s, 6H, CH$_3$), 0.86 (s, 9H, Bu^t).^{13}C NMR (C_6D_6, 100.6 MHz, 298 K, ppm): δ 190.7 (CN).

Synthesis of 15. To a THF (−10 °C) suspension of **6**·thf (0.63 g, 0.92 mmol) was added pyridine (0.10 mL, 1.2 mmol), and the reaction mixtured stirred overnight to give a red solution. The solution was filtered and solvent removed to 10 mL in vacuo. *n*-Hexane was added, and the microcrystalline product filtered and dried in vacuo (0.41 g, 57%). Anal. Calcd for $C_{40}H_{37}N_5$Ru: C, 69.75; H, 5.41; N, 10.17. Found: C, 68.89; H, 6.02; N, 9.63. ^{1}H NMR (C_6D_6, 400 MHz, 298 K, ppm): δ 8.75 (d, 2H, J = 4.4 Hz, py), 7.11–6.91 (m, 11H, Ar+py), 6.39–6.35 (m, 10H, Ph), 4.53 (s, 2H, CH), 1.98 (s, 12H, CH$_3$). ^{13}C NMR (C_6D_6, 100.6 MHz, 298 K, ppm): δ 300.6 (C carbene), 162.5.

Synthesis of 16. To a cooled (−10 °C) THF solution of **7** (0.73 g, 1.4 mmol) was added pyridine (0.22 mL, 2.7 mmol). The solution was allowed to warm to room temperature and stirred overnight. Solvent was removed in vacuo to 10 mL, and *n*-hexane (20 mL) added. The purple microcrystalline solid was filtered and dried in vacuo (0.45 g, 54%). Anal. Calcd for [Ru-(tmtaa)(CHPh)(Py)], $C_{34}H_{33}N_5$Ru: C, 66.65; H, 5.43; N, 11.43. Found: C, 65.81; H, 5.01; N, 10.95. ^{1}H NMR (C_6D_6, 400 MHz, 298 K, ppm): δ 18.3 (s, 1H, CH carbene); 8.73 (s, 2H, py); 8.12 (d, J = 7.3 Hz, 1H, py); 7.27–6.53 (m, 15H, Ar+py); 4.15 (s, 2H, CH); 1.92 (s, 12H, CH$_3$). ^{13}C NMR (C_6D_6, 100.6 MHz, 298 K, ppm): δ 296.3 (CH carbene).

Synthesis of 17. To a cooled (−20 °C) THF solution of **8** (0.84 g, 1.41 mmol) was added pyridine (0.12 mL, 1.4 mmol). The solution was allowed to warm to room temperature and then stirred for 5 h. The solvent was then removed in vacuo to 10 mL, and *n*-hexane (15 mL) added. The orange product was filtered and dried in vacuo (0.42 g, 44.4%). Anal. Calcd for [Ru(tmtaa){C(Ph)(COOMe)}(Py)], $C_{36}H_{35}N_5O_2$Ru: C, 64.46; H, 5.26; N, 10.44. Found: C, 64.24; H, 5.33; N, 10.32. ^{1}H NMR (C_6D_6, 400 MHz, 298 K, ppm): δ 8.88 (m, 2H, py); 8.03 (d, J = 7.2 Hz, 1H, py); 7.26–7.15 (m, 4H, Ar); 6.87–6.54 (m, 11H, Ar+py); 4.39 (s, 2H, CH); 3.51 (s, 3H, MeO); 2.08 (s, 12H, CH$_3$). ^{13}C NMR (C_6D_6, 100.6 MHz, 298 K, ppm): δ 285.6 (C carbene).

Synthesis of 18. To a cooled (−30 °C) stirred red toluene suspension (150 mL) of **7** (1.35 g, 2.54 mmol) was added a thf solution (30 mL) of PMe$_3$ (0.39 g, 5.08 mmol). The suspension was allowed to warm to room temperature and stirred overnight. The resulting green solution was concentrated to 20 mL, and *n*-hexane (30 mL) added. The green microcrystalline product was filtered and dried in vacuo (0.87 g, 58%). This complex was analyzed as [Ru(tmtaa)(PMe$_3$)$_2$]. A GC analysis of the mother liquor showed the presence of *cis*- and *trans*-

stilbene (86%, 14%). Anal. Calcd for [Ru(tmtaa)(PMe$_3$)$_2$], $C_{28}H_{40}N_4P_2$Ru: C, 56.46; H, 6.77; N, 9.41. Found: C, 55.59; H, 7.01; N, 9.30. ^{1}H NMR (C_6D_6, 200 MHz, 298 K, ppm): δ 6.75–6.70 (m, 4H, Ar); 6.41–6.36 (m, 4H, Ar); 4.11 (s, 2H, CH); 1.87 (s, 12H, CH$_3$); 1.37 (t, 18H, Me$_3$). ^{31}P[^{1}H] NMR (C_6D_6, 81 MHz, 298 K, ppm): δ 4.02.

Synthesis of 19. To a cooled (−20 °C) toluene suspension of **8** (0.46 g, 0.78 mmol) was added a THF solution of PMe$_3$ (0.06 g, 0.78 mmol). The suspension turned yellow and, on warming to room temperature, dissolved to give a green solution. Solvent was removed to dryness, and *n*-hexane (30 mL) added. The green precipitate was filtered and dried in vacuo (0.25 g, 48%). The product was recrystallized in toluene/ *n*-hexane. Anal. Calcd for **19**, $C_{34}H_{39}N_4O_2P_1$Ru: C, 61.16; H, 5.89; N, 8.39. Found: C, 60.42; H, 6.18; N, 8.24. IR (Nujol, ν_{max}/cm^{-1}): 1728 (s, COO), 1603 (m).^{1}H NMR (C_6D_6, 400 MHz, 298 K, ppm): δ 7.78–6.40 (m, 13H, Ar); 5.13 (s, 1H, HC=C); 4.23 (s, 1H, CH); 3.43 (s, 3H, OCH$_3$); 2.10 (s, 6H, CH$_3$); 2.02 (s, 6H, CH$_3$), 1.11 (s, 9H, Me$_3$).^{31}P[^{1}H] NMR (C_6D_6, 81 MHz, 298 K, ppm): δ 0.54.

X-ray Crystallography for Complexes 5, 6, 11, and 12 in Their Solvated Form. Crystals of **5**, **6**, **11**, and **12** were mounted in glass capillaries and sealed under nitrogen. Intensity data for all four complexes were collected on a Rigaku AFC7 single-crystal diffractometer by using graphite-monochromated Mo Kα radiation (λ = 0.7107 Å). Crystal data are reported in Table 1. The intensities were corrected for Lorentz and polarization factors. No absorption correction was applied. The structures were solved by conventional Patterson and Fourier methods and refined through full-matrix least-squares methods. The non-hydrogen atoms were treated anisotropically. The hydrogen atoms, located on positive regions of the difference Fourier maps, were added as fixed contributions at their calculated positions. In both **5** and **11** the Fourier maps showed that one molecule of toluene was located around an inversion center, with half-occupancy of the methyl group. Complex neutral-atom scattering factors, including anomalous dispersion terms for all non-H atoms, were taken from International Tables for X-ray Crystallography.[13] Calculations were carried out by using SHELX93.[14] Final non-H positional parameters, anisotropic thermal parameters, H atom coordinates, and tables of all bond lengths and angles are available as Supporting Information.[15]

Results and Discussion

(a) Ruthenium–tmtaa Derivatives. For the purposes of this study we found [{Ru(tmtaa)}$_2$(μ-C$_8$H$_{12}$)], **1**, to be the most appropriate starting material in that its preparation is straightforward, high yielding, and involves the labile olefin ligand. The synthesis of **1** and its conversion to other [Ru(tmtaa)] derivatives is outlined in Scheme 1.

The NMR characterization of **1** was not possible in noncoordinating solvents due to its insoluble nature, whereas spectra recorded in pyridine actually corresponded to that of **2**. Complexes **2**–**5** display a common pattern in the ^{1}H NMR spectrum with a singlet for the *meso*-imino protons and a singlet for the four methyls, which are also the most sensitive to conformational changes of the tmtaa ligand. The C–O and C–N stretching vibrations are diagnostic of the electron density at the metal. Surprisingly low C–O [1904 cm^{-1} in **3**] and C–N [1920 cm^{-1} in **4** vs 2134 cm^{-1} in free

(13) *International Tables for X-ray Crystallography*; Kynoch Press: Birmingham, England, 1974; Vol. IV.
(14) Sheldrick, G. M. *SHELXL-93, Program for Crystal Structure Refinement*; University of Göttingen, Göttingen, Germany, 1993.
(15) See paragraph at the end regarding Supporting Information.

Table 1. Crystal Data and Structure Refinement for 5, 6, 11, and 12

	5	**6**	**11**	**12**
chem formula	$C_{32}H_{40}N_6Ru\cdot0.5C_7H_8$	$C_{35}H_{32}N_4Ru\cdot C_4H_8O$	$C_{32}H_{30}N_4O_3Ru\cdot1.5C_7H_8$	$C_{31}H_{28}N_4O_2Ru\cdot C_7H_8$
fw	655.84	681.82	757.37	681.78
temp, K	143(2)	143(2)	143(2)	293(2)
cryst syst	triclinic	triclinic	monoclinic	triclinic
space group	$P\bar{1}$	$P\bar{1}$	$P2_1/c$	$P\bar{1}$
a, Å	12.481(4)	11.414(14)	11.269(4)	10.617(5)
b, Å	13.145(3)	14.297(12)	9.445(2)	19.436(10)
c, Å	10.587(3)	11.332(8)	33.854(12)	8.378(3)
α, deg	96.87(2)	108.77(6)	90	90.34(4)
β, deg	101.76(2)	104.29(10)	91.63(3)	104.24(3)
γ, deg	103.65(2)	105.25(11)	90	80.99(4)
V, Å^3	1626.5(8)	1574(3)	3602(2)	1654.1(13)
Z	2	2	4	2
D_{calc}, g/cm^3	1.339	1.439	1.397	1.369
μ, mm^{-1}	0.516	0.537	0.481	0.513
$F(000)$	686	708	1570	704
indep refls	5839	5843	4987	7245
GOF^a	0.993	1.030	1.896	1.017
R^b [$I > 2\sigma(I)$]	0.039	0.088	0.036	0.046
wR2^c [$I > 2\sigma(I)$]	0.097	0.222	0.112	0.107

^{a} GOF = $[\Sigma w(|F_o| - |F_c|)^2/(\text{no. obser} - \text{no. variab})]$. ^{b} R = $\Sigma|\Delta F|/\Sigma|F_o|$. ^{c} wR2 = $[\Sigma(w\Delta F^2)^2/\Sigma(wF_o^2)^2]^{1/2}$.

Scheme 1
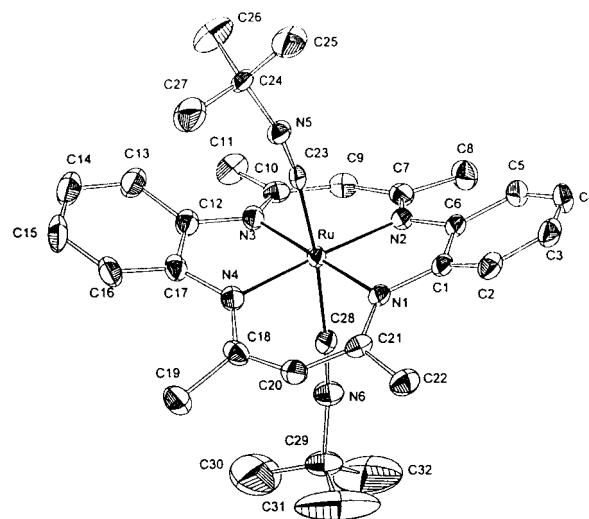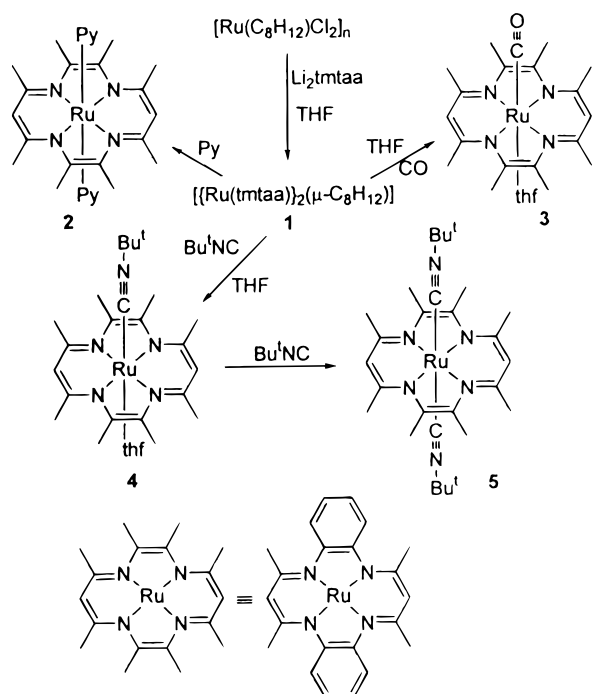
Figure 1. ORTEP drawing (thermal ellipsoid 50% probability) of complex **5**.

Bu^{t}NC] bands were observed for complexes **3** and **4**, and this is indicative of high electron density and an efficient π-back-bonding to the ligand. The displacement of the equatorial thf in **3** and **4** by a further molecule of ligand was successful only for **4**. Unlike ruthenium–porphyrin chemistry, we did not observe the formation of a dicarbonyl like [Ru(TPP)(CO)$_2$], though in the latter case the second CO is extremely labile and was lost even under a N$_2$ atmosphere.[16] The obtention of **5** [ν_{CN}, 2091 cm^{-1}] is related to the greater σ-donating and lower π-acidic nature of the isocyanide ligand. In all [M(t-mtaa)L$_2$] species, the arrangement of the two L ligands can be either cis or trans, depending on the degree that the metal is out of the N$_4$ plane, and is a direct consequence of the d^n configuration.[2d] In the case of metals with a low-spin d^6 configuration, the arrange-
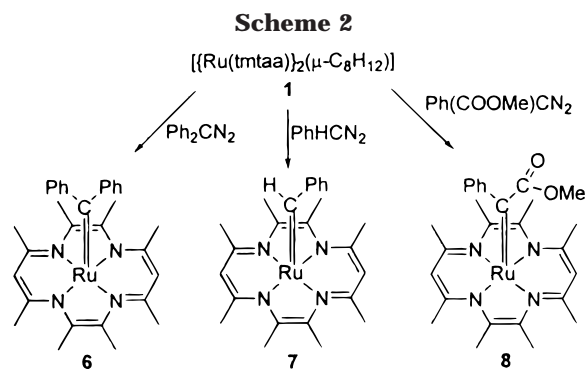
ment is almost exclusively trans, as confirmed by X-ray analyses. Due to the particular focus of this paper on the Ru–C multiple bond, only the X-ray analysis of **5** will be reported. The structure of **5** is displayed in Figure 1, with a list of the corresponding selected parameters in Table 2. Although the metal is hexaco-ordinate, unlike the phosphine derivatives [Ru(tmtaa)-(PR$_3$)$_2$],[4,5] the ligand has a slight saddle shape confor-mation, with the arene substituents tilted up in the C23 direction and the diiminato rings on the opposite side, the dihedral angles with the N$_4$ plane being 18.0(1)°, 22.2(3)°, and 12.3(3)°, 19.8(1)°, respectively. The metal out-of-plane distance [0.026(2) Å] is not particularly informative in the case of hexacoordinate [M(tmtaa)L$_2$] complexes. The structural parameters related to the [Ru(tmtaa)] fragment show the usual trend.[2] A signifi-cant difference has been observed between Ru–C23 [1.980(4) Å] and Ru–C28 [2.013(4) Å] according to a different steric environment for the two isonitriles. Such Ru–C bond distances are significantly longer than those in the analogous porphyrin complex [Ru(TPP)(Bu^{t}NC)$_2$] [Ru–C$_{av}$, 1.901(3) Å].[17] The deviation of the Ru–C–N (isonitrile) fragment from linearity occurs almost *nor-*

(16) Eaton, G. R.; Eaton, S. S. *J. Am. Chem. Soc.* **1975**, *97*, 235.

Table 2. Selected Geometrical Parameters for 5 and 6: Bond Lengths and Metal Out-of-Plane Distances (d)[a] Are in Angstroms; Bond and Dihedral (α and β)[b] Angles in Degrees

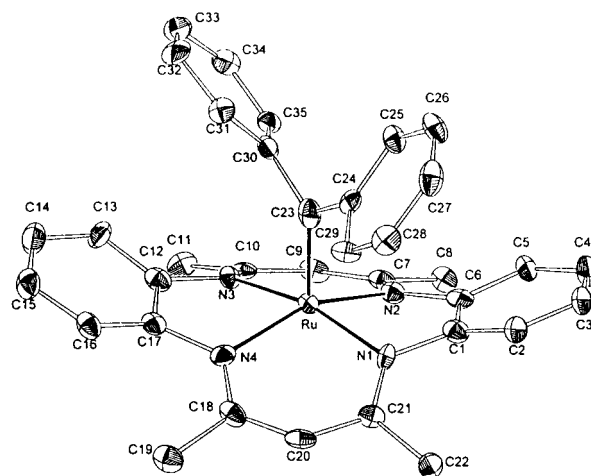|	5	6		5	6
Ru−C(23)	1.980(4)	1.874(8)	N(3)−C(10)	1.324(5)	1.331(9)
Ru−C(28)	2.013(4)		N(3)−C(12)	1.409(5)	1.432(9)
Ru−N(1)	2.032(3)	2.044(6)	N(4)−C(18)	1.338(5)	1.356(10)
Ru−N(2)	2.035(3)	2.024(6)	N(4)−C(17)	1.394(5)	1.426(9)
Ru−N(3)	2.040(3)	2.034(6)	N(5)−C(23)	1.155(5)	
Ru−N(4)	2.038(4)	2.028(7)	N(5)−C(24)	1.453(5)	
N(1)−C(21)	1.334(5)	1.333(9)	N(6)−C(28)	1.149(5)	
N(1)−C(1)	1.411(5)	1.417(9)	N(6)−C(29)	1.460(5)	
N(2)−C(7)	1.333(5)	1.351(10)	C(23)−C(24)		1.489(10)
N(2)−C(6)	1.414(5)	1.426(9)	C(23)−C(30)		1.495(10)
C(23)−Ru−C(28)	173.9(2)		C(1)−N(1)−Ru	112.2(2)	110.4(5)
C(23)−Ru−N(1)	92.94(14)	98.1(3)	C(7)−N(2)−C(6)	128.8(3)	127.1(6)
C(28)−Ru−N(1)	88.57(14)		C(7)−N(2)−Ru	118.9(3)	121.2(5)
C(23)−Ru−N(2)	94.79(14)	102.4(3)	C(6)−N(2)−Ru	112.3(3)	111.6(5)
C(28)−Ru−N(2)	91.31(14)		C(10)−N(3)−C(12)	128.8(4)	126.7(6)
N(1)−Ru−N(2)	81.83(13)	80.2(3)	C(10)−N(3)−Ru	119.1(3)	121.7(5)
C(23)−Ru−N(3)	86.84(14)	97.4(3)	C(12)−N(3)−Ru	112.1(3)	110.9(5)
C(28)−Ru−N(3)	91.58(14)		C(18)−N(4)−C(17)	129.1(4)	126.6(6)
N(1)−Ru−N(3)	179.35(14)	164.5(2)	C(18)−N(4)−Ru	118.3(3)	121.4(5)
N(2)−Ru−N(3)	98.80(14)	96.7(3)	C(17)−N(4)−Ru	112.4(3)	112.0(5)
C(23)−Ru−N(4)	88.35(14)	101.6(3)	C(23)−N(5)−C(24)	168.0(4)	
C(28)−Ru−N(4)	85.55(14)		C(28)−N(6)−C(29)	168.5(4)	
N(1)−Ru−N(4)	98.57(14)	96.4(3)	N(5)−C(23)−Ru	171.9(3)	
N(2)−Ru−N(4)	176.81(13)	156.0(2)	N(6)−C(28)−Ru	172.8(4)	
N(3)−Ru−N(4)	80.81(14)	80.2(3)	C(24)−C(23)−Ru		122.5(5)
C(21)−N(1)−C(1)	128.9(3)	126.4(6)	C(30)−C(23)−Ru		122.3(5)
C(21)−N(1)−Ru	118.8(3)	121.9(5)			
α₁	18.0(1)	18.1(3)	α₂	22.2(1)	19.0(3)
β₁	12.3(2)	25.8(5)	β₂	19.7(1)	29.9(3)
d	0.026(2)	0.347(3)			

[a] Distance of Ru atom from N_4 donor plane. [b] Dihedral angles between N_4 donor plane and C1···C6 benzenoid ring = α_1; between N_4 and C12···C17 benzenoid ring = α_2; between N_4 and C7···C11 carbons of pentanediiminate ring = β_1; between N_4 and C18···C22 pentanediiminate ring = β_2.

Scheme 2

$[\{Ru(tmtaa)\}_2(\mu\text{-}C_8H_{12})]$

1

Ph₂CN₂ → **6** ; PhHCN₂ → **7** ; Ph(COOMe)CN₂ → **8**

Figure 2. ORTEP drawing (thermal ellipsoid 50% probability) of complex **6**.

mally in isonitrile derivatives (Table 2). Larger distortions were observed for the porphyrin complex and are explained by crystal packing influences.[17]

(b) Ruthenium−tmtaa−Carbene Complexes. The synthesis of ruthenium−carbene functionalities bonded to a macrocyclic ligand is displayed in Scheme 2. The carbene derivatives **6**−**8** have been obtained by reacting a THF suspension of **1** with the corresponding diazoalkane, preferably at −20/−30 °C. The reaction produces crystalline solids in good yield. These species were easily characterized by their low-field ¹³C signals, indicative of a coordinated carbene: 291.8 ppm for **6** and 279.2 ppm for **8**. Although the corresponding signal was not seen for complex **7**, the ¹H NMR did show a characteristic low-field signal centered at 17.1 ppm for the carbene proton. This deshielding of the carbene signal was explained by invoking the presence of low-energy

electronic excited states, which results in a large paramagnetic contribution to the chemical shift.[18] The tmtaa ligand has the usual ¹H NMR spectrum with a singlet for the meso-protons and the methyl groups.

The structure of a ruthenium−carbene functionality, complex **6** containing THF of crystallization, is displayed in Figure 2, with selected bond distances and angles in Table 2. The coordination environment of ruthenium is a distorted tetragonal pyramid, unlike that in carbene−Fe,[19] carbene−Os,[20] and carbene−Rh[21] porphyrins, where

(17) Jameson, J. B.; Ibers, J. A. *Inorg. Chem.* **1979**, *18*, 1200.

(18) Crabtree, R. H. *The Organometallic Chemistry of the Transition Metals*, 2nd ed.; Wiley: New York, 1994; Chapter 11.

Scheme 3

Scheme 4
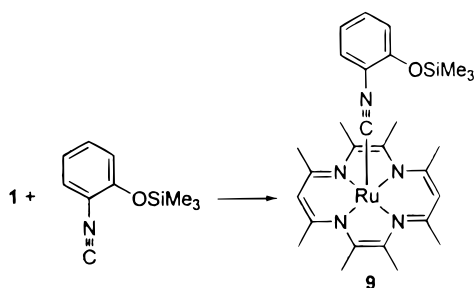
the metal is always hexacoordinate. The metal is displaced by 0.374(3) Å from the N_4 average plane toward the carbene carbon. The Ru–C23 vector is perpendicular to the N_4 core. The carbene C23,C24,C30 plane is almost parallel to the N1–N3 vector, the torsional angles C30,C23,Ru,N3 and C24,C23,Ru,N2 being −6.6(6)° and −91.0(6)°, respectively. The Ru=C bond distance [1.874(8) Å], which does not have any reference in Ru–porphyrin or macrocyclic chemistry, is rather close to those found in Ru–phosphine derivatives.[7,22] The question of whether the oxidation state of Ru in **6** is II or IV can be reasonably answered by considering the Ru distance from the N_4 plane.[23] The value found in the present case [0.347(3) Å]) is that expected for a low-spin d^6, compared with 0.216(5) Å in [Ru(tmtaa)(CO)(thf)], **3**.[24] A much longer distance would be expected for a d^4 configuration. The tmtaa ligand has the usual saddle shape conformation.[2]

Two other synthetic approaches have been tried in order to get the Ru–carbene functionality bonded to a macrocycle. The first one involves reacting **1** with an electron-rich alkene such as bis(1,3-diphenylimidazolidinylidene-2). Attempts to initiate the C–C scission in refluxing THF or toluene were unsuccessful, as strictly no reaction occurred. In contrast, it has been reported that [RuCl$_2$(PPh$_3$)$_3$] reacts with the same electron-rich alkene under similar conditions to form the surprising tetracarbene *trans*-dichlorotetrakis (1,3-diphenylimidazolidinylidene-2) ruthenium(II).[25] The second strategy is based on the reaction of coordinated isonitriles with nucleophiles and more specifically on the work of Hahn and co-workers.[26] The formation of the isonitrile complex **9** occurs easily (Scheme 3). The characteristic IR(CN) band at 1997 cm^{-1} and the ^{13}C NMR at 208.8 ppm are typical of a coordinated isonitrile. The hydrolysis of the Si–O bond was done in MeOH and resulted in a mixture of poorly defined
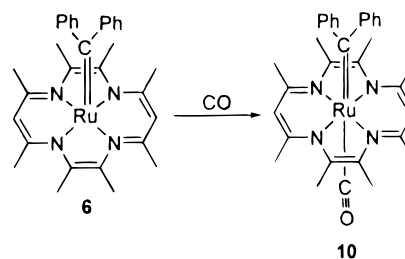
products. Alkylation of this material with MeI does not lead to the desired carbene, but partially to the corresponding methoxy-functionalized isonitrile complex. This synthetic approach was unsuccessful due to the very low electrophilicity of the isocyanide carbon bonded to the unexpectedly electron-rich ruthenium. Theoretical calculations (vide infra), in fact, suggest an abnormal negative charge on the metal, as expected for a d^8 rather than for a d^6 configuration.

(c) Ligand-Induced Labilization of the Ru–Carbene Functionality. The carbene complexes **6**–**8** are particularly thermally stable, but they undergo easy labilization by a *trans*-incoming ligand under the condition that it has an appropriate balance between σ-donating and π-accepting binding properties. As a matter of fact, they are particularly sensitive to ligands such as CO, RNC, and PR$_3$, but not to pyridine. When solutions of **6**–**8** are reacted with carbon monoxide (1 atm) at room temperature and in THF solution, three different reaction pathways are observed, depending on the substituents on the carbene carbon.

In the case of **6**, complex **10** was isolated (see Scheme 4), which corresponds to the simple coordination of carbon monoxide trans to the diphenylcarbene fragment. No color changes were observed in the reaction of **6** with CO, but a typical IR band at 1906 cm^{-1} and the ^{13}C NMR peak at 270.9 ppm confirm the coordination of CO. Surprisingly, the chemical shift of the carbene carbon signal is virtually unaffected. In the case of **10**, the very low CO stretching frequency is indicative of an electron-rich [Ru(tmtaa)] fragment and indirectly supports (vide infra) the terminology we use for such Ru derivatives, namely, that of a carbene, instead of an alkylidene.

In the case of **7** and **8**, the reaction proceeds behind the simple coordination. The trans carbon monoxide labilizes the carbene, causing its migration to the macrocycle with a quite different synthetic result, depending on the substituents R and R′. In the case of R = Ph, R′ = COOMe (complex **8**, Scheme 5) we can suppose the labilized carbene carbon bridging the metal and the meso-carbon. A bridging bonding mode of the carbene carbon, like that observed between iron and one of the nitrogens of the porphyrin,[27] is, however, prevented by the distance between the metal and the meso-

(19) Mansuy, D.; Lange, M.; Chottard, J. C.; Bartoli, J. F.; Chevrier, B.; Weiss, R. *Angew. Chem.* **1978**, *90*, 828.

(20) Djukic, J.-P.; Smith, D. A.; Young, V. G., Jr.; Woo, L. K. *Organometallics* **1994**, *13*, 3020.

(21) Boschi, T.; Licoccia, S.; Paolesse, R.; Tagliatesta, P. *Organometallics* **1989**, *8*, 330.

(22) (a) Schwab, P.; Grubbs, R. H.; Ziller, J. W. *J. Am. Chem. Soc.* **1996**, *118*, 100. (b) Esteruelas, M. A.; Lahoz, F. J.; Oñate, E.; Oro, L. A.; Zeier, B. *Organometallics* **1994**, *13*, 4258.
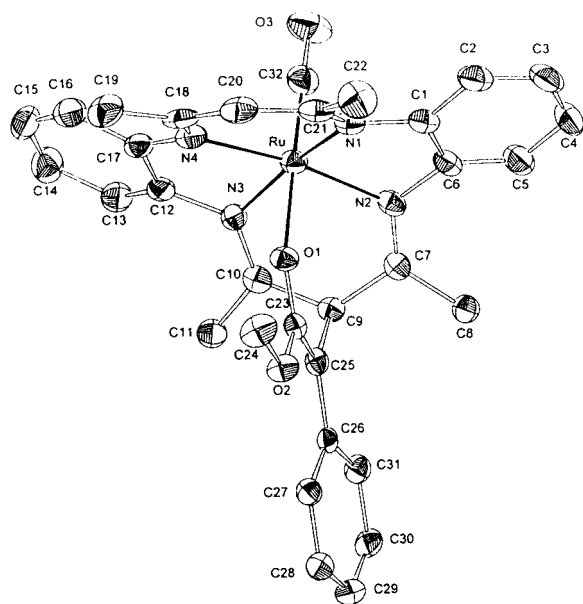
(23) A correlation in tmtaa complexes has been established between the out-of-plane distance of the metal and its d^n configuration: see ref 2d.

(24) Unpublished results.

(25) Hitchcock, P. B.; Lappert, M. F.; Pye, P. L. *J. Chem. Soc., Dalton Trans.* **1978**, 826. Hitchcock, P. B.; Lappert, M. F.; Pye, P. L. *J. Chem. Soc., Chem. Commun.* **1976**, 644.
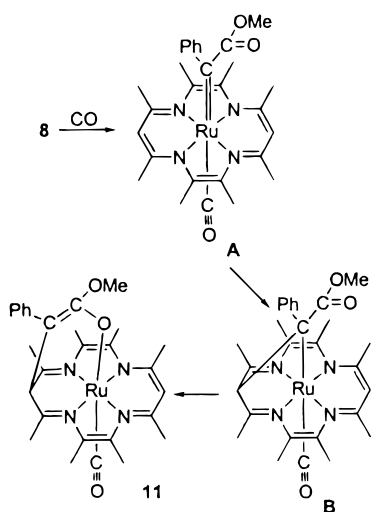
(26) Hahn, F. E.; Tamm, M. *Organometallics* **1995**, *14*, 2597. Hahn, F. E.; Tamm, M.; Lügger, T. *Angew. Chem., Int. Ed. Engl.* **1994**, *33*, 1356. Hahn, F. E.; Tamm, M. *J. Organomet. Chem.* **1993**, *456*, C11. Hahn, F. E. *Angew. Chem, Int. Ed. Engl.* **1993**, *32*, 650.

(27) (a) Brothers, P. J.; Collman, J. P. *Acc. Chem. Res.* **1986**, *19*, 209. (b) Mansuy, D. *Pure Appl. Chem.* **1987**, *59*, 759. (c) Artaud, I.; Gregoire, N.; Battioni, J.-P.; Dupre, D.; Mansuy, D. *J. Am. Chem. Soc.* **1988**, *110*, 8714. (d) Artaud, I.; Gregoire, N.; Leduc, P.; Mansuy, D. *J. Am. Chem. Soc.* **1990**, *112*, 6899. (e) Mansuy, D.; Mahy, J. P. In *Metalloporphyrins Catalyzed Oxidations*; Montanari, F., Casella, L., Eds.; Kluwer: Dordrecht, The Netherlands, 1994; pp 175–206. (f) Latos-Grazynski, L.; Cheng, R.-J.; La Mar, G. N.; Balch, A. L. *J. Am. Chem. Soc.* **1981**, *103*, 4270. (g) Balch, A. L.; Cheng, R.-J.; La Mar, G. N.; Latos-Grazynski, L. *Inorg. Chem.* **1985**, *24*, 2651.

C9,C10,N3 with C9 displaced 0.315(4) Å out of the N2, C7,C10,N3 plane. As a consequence, C7−N2 [1.270(5) Å] and C10−N3 [1.278(5) Å] become imino groups and the meso-alkylated tmtaa now functions as a monoanionic ligand. The bonding sequence shown for the bridge across the sp³ C9 and Ru in Scheme 5 is supported by (i) the C23−C25 [1.390(5) Å] double-bond character; (ii) the planarity of the bridge, the C23−C25−C26−C27 having a torsional angle of −7.8(6)°; and (iii) some lengthening of the C23−O1 [1.260(4) Å] bond, which is in agreement with a charge delocalization over the O1−C23−C25 fragment functioning as a monoanionic oxoallyl moiety. The modified tmtaa in **11** maintains the saddle shape conformation with the two phenyl groups tilted up in the same direction as the Ru−CO vector. This is always the case when one of the axial ligands is multiple bonded to the metal [see complex **6** and [Ru-(tmtaa)(CO)(thf)], **3**]. The Ru−C32 [1.793(5) Å] bond distance is close to that in **3** [1.761(6) Å] and significantly shorter than that found in other octahedral Ru-(II) complexes having an oxygen donor ligand trans to CO.[29]

The reaction pathway of **7** upon labilization by carbon monoxide (see Scheme 6) involves, in its preliminary stage, the migration of the carbene carbon to a C=C bond of the diiminato ring. This step is followed by a hydrogen shift to form the seven-membered metallacycle (see complex **12**), within the metal−macrocycle moiety. The resulting novel macrocycle, which becomes conformationally more flexible, rearranges around the metal and leaves two cis coordination sites available for carbon monoxide. The ¹H NMR of complex **12** shows a significant loss of symmetry. The methyl groups are no longer equivalent and show four signals. Apart from the aromatic region, one singlet and two doublets, each integrating as one proton, are observed. The DEPT and proton−carbon correlation experiments clearly show that a CH₂ unit was formed, which corresponds to the two previous doublets. Supporting evidence is given by the IR, which shows two characteristic CO bands at 2016 and 1948 cm⁻¹, and by the two ¹³C NMR signals at 199.8 and 197.5 ppm. It should be mentioned, at this stage, that although in a different context, migration of alkyl groups from the metal to the imino carbons of the macrocycle ligand tmtaa has been observed in the [Zr(tmtaa)]²f and [Nb(tmtaa)] organometallic chemistry.[30] The proposed bonding scheme for **12** is confirmed by the structural parameters (Table 4) related to the structure of **12** shown in Figure 4. The new macrocyclic ligand contains two five-membered, one six-membered, and one seven-membered ring. In the last mentioned ring, the nitrogen donor atom N1 becomes an imido group with the related sp³ geometry and a short Ru−N1 distance [2.060(5) Å], while the neutral imino sp² nitrogen N4 binds Ru with a long distance [Ru−N4, 2.223(5) Å]. The two cis-arranged CO experience a different trans influence by N2 and N4; thus, the longer Ru−C30 bond [1.882(6) Å] is trans to an amino and the shorter Ru−C31 [1.833(6) Å] to an imido group.

The reaction of **7** and **8** with ButNC parallels the reaction with carbon monoxide, and due to the close

Figure 3. ORTEP drawing (thermal ellipsoid 50% probability) of complex **11**.

Scheme 5

carbon. Therefore, the attack at the meso-carbon by the carbene is followed by a rearrangement of the carbene fragment to a geometrically more appropriate bridging unit, such as the one in complex **11**. A structural analogue can be found in cobalt(III)−tmtaa chemistry, where a vinyl group bridges the metal and the macrocyclic ligand.[28] Complex **11** shows a partial loss of symmetry in its ¹H NMR spectrum. Two important features are observed. First, there are only two signals for the CH₃ groups integrating for 6H each, implying a mirror plane in the molecule. Second, there are two different CH peaks, which also imply a new chemical environment. A single CO band was detected by IR (1905 cm⁻¹) and ¹³C NMR (211.9 ppm) spectra. The structure of **11** is shown in Figure 3, and its selected parameters are given in Table 3. The transfer of the carbene carbon to C9 removes the aromaticity and the planarity of the six-membered metallacycle Ru,N2,C7,

(28) Weiss, M. C.; Goedken, V. L. *J. Am. Chem. Soc.* **1976**, *98*, 3389. Weiss, M. C.; Gordon, G. C., Goedken, V. L. *J. Am. Chem. Soc.* **1979**, *101*, 857.

(29) Alessio, E.; Milani, B.; Bolle, M.; Mestroni, G.; Faleschini, P.; Todone, F.; Geremia, S.; Calligaris, M. *Inorg. Chem.* **1995**, *34*, 4722, and references therein.

(30) Unpublished results.

Table 3. Selected Geometrical Parameters for 11: Bond Lengths and Metal Out-of-Plane Distances (d)[a] Are in Angstroms; Bond and Dihedral (α and β)[b] Angles in Degrees

Ru−C(32)	1.793(5)	O(3)−C(32)	1.165(5)	N(4)−C(18)	1.340(5)
Ru−N(1)	2.011(3)	N(1)−C(21)	1.318(5)	N(4)−C(17)	1.408(5)
Ru−N(2)	2.024(3)	N(1)−C(1)	1.417(5)	C(7)−C(9)	1.518(5)
Ru−N(3)	2.006(3)	N(2)−C(7)	1.270(5)	C(9)−C(10)	1.529(6)
Ru−N(4)	2.027(3)	N(2)−C(6)	1.428(5)	C(9)−C(25)	1.538(5)
Ru−O(1)	2.134(3)	N(3)−C(10)	1.278(5)	C(23)−C(25)	1.387(5)
O(1)−C(23)	1.260(4)	N(3)−C(12)	1.429(5)	C(25)−C(26)	1.453(5)
O(2)−C(23)	1.368(4)				
C(32)−Ru−N(3)	95.6(2)	N(3)−Ru−O(1)	84.51(12)	C(6)−N(2)−Ru	111.9(2)
C(32)−Ru−N(1)	95.3(2)	N(1)−Ru−O(1)	84.58(12)	C(10)−N(3)−C(12)	127.1(3)
N(3)−Ru−N(1)	169.08(13)	N(2)−Ru−O(1)	83.22(11)	C(10)−N(3)−Ru	118.8(3)
C(32)−Ru−N(2)	96.0(2)	N(4)−Ru−O(1)	86.56(11)	C(12)−N(3)−Ru	111.8(2)
N(3)−Ru−N(2)	98.94(13)	C(23)−O(1)−Ru	137.2(2)	C(18)−N(4)−C(17)	128.2(4)
N(1)−Ru−N(2)	80.36(13)	C(21)−N(1)−C(1)	128.1(4)	C(18)−N(4)−Ru	119.5(3)
C(32)−Ru−N(4)	94.2(2)	C(21)−N(1)−Ru	119.3(3)	C(17)−N(4)−Ru	112.1(3)
N(3)−Ru−N(4)	80.32(13)	C(1)−N(1)−Ru	112.1(2)	C(7)−C(9)−C(10)	127.4(3)
N(1)−Ru−N(4)	98.40(13)	C(7)−N(2)−C(6)	125.7(4)	C(7)−C(9)−C(25)	105.7(3)
N(2)−Ru−N(4)	169.77(13)	C(7)−N(2)−Ru	120.1(3)	C(10)−C(9)−C(25)	105.6(3)
C(32)−Ru−O(1)	179.2(2)				
α_1	18.4(2)	α_2	18.8(2)	β_1	27.1(2)
β_2	24.4(3)				
d	0.186(2)				

[a] Distance of Ru atom from N_4 donor plane. [b] Dihedral angles between N_4 donor plane and C1···C6 benzenoid ring = α_1; between N_4 and C12···C17 benzenoid ring = α_2; between N_4 and C7, C8, C10, C11 = β_1; between N_4 and C18···C22 carbons of pentanediiminate ring = β_2.
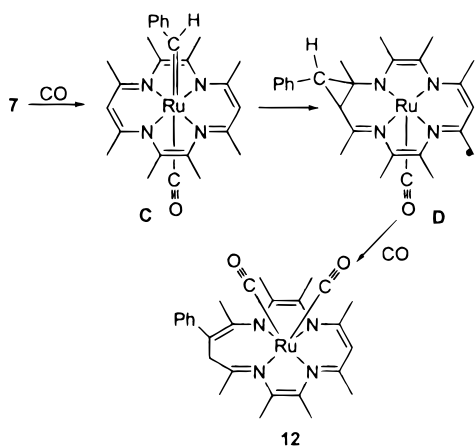
Scheme 6

relationship between CO and RNC in terms of σ and π properties, we suppose that the reactions follow the same pathway displayed in Schemes 5 and 6. When complex **7** was reacted with 2 equiv of Bu^{t}NC (see Scheme 7), complex **13** was obtained as a crystalline green material. NMR evidence implies that its structure is similar to complex **12** (Scheme 7). Similarly, four signals were observed for the methyl groups of the tmtaa due to the loss of symmetry in the ligand, further supported by two Bu^t peaks at 0.96 and 0.82 ppm. The DEPT and the ^{1}H−^{13}C correlation experiments confirmed the presence of a CH$_2$ group, which appeared as two doublets in the ^{1}H NMR. We note that they are particularly more deshielded than in complex **12**. When **8** was reacted with Bu^{t}NC in toluene, complex **14** slowly formed (Scheme 7). The ^{1}H NMR spectrum is similar to complex **11** with an additional peak corresponding to the Bu^t group. Only slight variations in the chemical shift were observed. An IR band centered at 1934 cm^{-1} and the ^{13}C NMR signals at 190.7 ppm characterized the single coordinated isonitrile. Complex **6** did not bind with Bu^{t}NC, due to the incompatibility between the high

electron density of the metal in **6** and the powerful σ-donor ability of Bu^{t}NC. We should mention at this stage that the balance between the σ-donor and π-acceptor properties of the axial ligand plays a major role in the activation of the carbene functionality, determining its labilization pathway. This can follow a free-radical type mechanism (Scheme 5) or a more carbene-like pathway (Scheme 6) (vide infra).

With the general aim of understanding the relevance of the σ-donor and π-acceptor properties of the axial ligand, we moved from carbon monoxide and isonitrile to pyridine and phosphines. The former choice was for a ligand having both a poor π-acceptor and not very strong σ-donating properties. Complexes **6**−**8** were converted into hexacoordinated ruthenium carbene derivatives **15**−**17** (Scheme 8) in the reaction with pyridine. The coordination of the sixth ligand trans to the carbene functionality did not cause any labilization of the carbene functionality, as it did in the case of CO and RNC. The presence of the pyridine ligand in complexes **15**−**17** was revealed by some significant shift in the ^{13}C resonance of the carbene carbon (see Experimental Section).

Phosphines are an excellent class of ligands for helping define the limits of the carbene labilization, being excellent σ-donors, good trans labilizing agents, and poor π-acceptors. Fine-tuning of the electronic properties can be achieved by the use, eventually, of different substituents at phosphorus. Therefore we reacted carbene complexes **6**−**8** with trimethylphosphine, which amounts to a decrease in the π-acidity and increase in the σ-basicity. Strictly no reaction occurred with the stable diphenylcarbene derivative **6**, in contrast with carbenes **7** and **8** (see Scheme 9). When complex **7** was reacted in toluene at −30 °C with 1 or 2 equiv of the corresponding phosphine, the bis(phosphine) compounds **18** formed as a green crystalline material, as confirmed by NMR spectroscopy and elemental analysis (Scheme 9). A GC analysis of the mother liquor showed

Table 4. Selected Bond Lengths (Å) and Angles (deg) for 12

|					
Ru−C(30)	1.882(6)	N(1)−C(1)	1.381(7)	N(4)−C(18)	1.289(7)
Ru−C(31)	1.833(6)	N(1)−C(28)	1.420(7)	N(4)−C(17)	1.441(7)
Ru−N(1)	2.060(5)	N(2)−C(7)	1.337(7)	C(18)−C(20)	1.502(9)
Ru−N(2)	2.102(4)	N(2)−C(6)	1.427(7)	C(20)−C(21)	1.537(8)
Ru−N(3)	2.078(5)	N(3)−C(10)	1.338(7)	C(21)−C(28)	1.344(8)
Ru−N(4)	2.223(5)	N(3)−C(12)	1.431(7)		
C(31)−Ru−C(30)	91.2(2)	C(31)−Ru−N(4)	173.4(2)	C(6)−N(2)−Ru	112.4(3)
C(31)−Ru−N(1)	92.0(2)	C(30)−Ru−N(4)	86.7(2)	C(10)−N(3)−C(12)	123.0(5)
C(30)−Ru−N(1)	96.5(2)	N(1)−Ru−N(4)	94.4(2)	C(10)−N(3)−Ru	124.4(4)
C(31)−Ru−N(3)	99.3(2)	N(3)−Ru−N(4)	74.8(2)	C(12)−N(3)−Ru	110.4(3)
C(30)−Ru−N(3)	96.3(2)	N(2)−Ru−N(4)	99.0(2)	C(18)−N(4)−C(17)	122.4(5)
N(1)−Ru−N(3)	162.7(2)	C(1)−N(1)−C(28)	118.9(5)	C(18)−N(4)−Ru	131.7(4)
C(31)−Ru−N(2)	83.4(2)	C(1)−N(1)−Ru	112.8(4)	C(17)−N(4)−Ru	105.7(3)
C(30)−Ru−N(2)	173.6(2)	C(28)−N(1)−Ru	115.0(4)	O(1)−C(30)−Ru	177.3(6)
N(1)−Ru−N(2)	80.3(2)	C(7)−N(2)−C(6)	124.7(5)	O(2)−C(31)−Ru	178.6(5)
N(3)−Ru−N(2)	87.9(2)	C(7)−N(2)−Ru	118.9(4)		
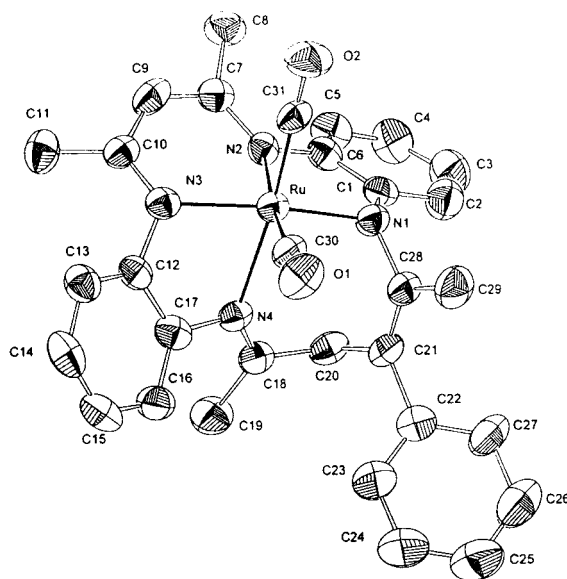
Figure 4. ORTEP drawing (thermal ellipsoid 50% probability) of complex **12**.

Scheme 7
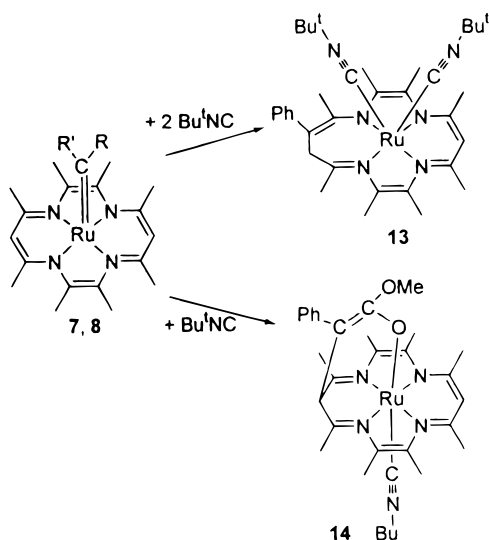
the presence of *cis*- and *trans*-stilbene, 86% and 14%, respectively. The reaction of **8** with PMe₃ in toluene led to **19**. Good analytical data were obtained for the recrystallized product. The increased complexity of the ¹H NMR spectrum implies a loss of symmetry similar to that observed for complexes **11** and **14**. The ¹H and

Scheme 8
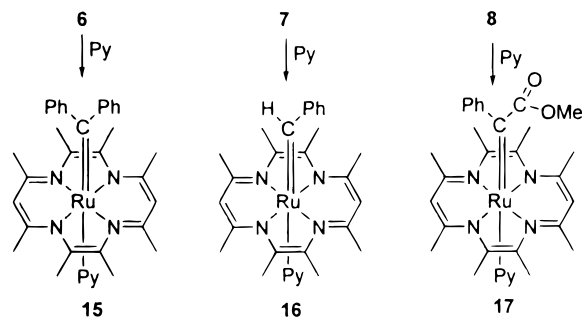
Scheme 9
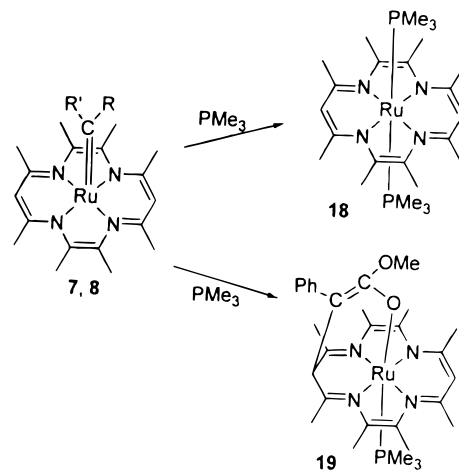
³¹P NMR spectra show singlets at 1.11 and 0.55 ppm, respectively, which corresponds to coordinated PMe₃. The ³¹P NMR signal of the free phosphine is at −62.0 ppm.[31] These data nicely support a structure similar to that observed for complexes **11** and **14**. The PMe₃ ligand, based on the results in Scheme 9, considerably affects the labilization pathway of the Ru−carbene functionality. First of all the absence of any reaction with **6** is in agreement with the poor π-acceptor properties and the strong σ-donor ability of the ligand, as we mentioned for the different reactivity of **6** toward CO and RNC. The formation of **18** and stilbenes from **7** would be understandable admitting that the labilization caused by a strong σ-donor like PMe₃ generates a free carbene. The formation of **19** from the reaction of **8** with

(31) Verkade, J. G.; Quin, L. D. *Phosphorus-31 NMR Spectroscopy in Stereochemical Analysis*; VCH: Berlin, 1987; Vol 8.
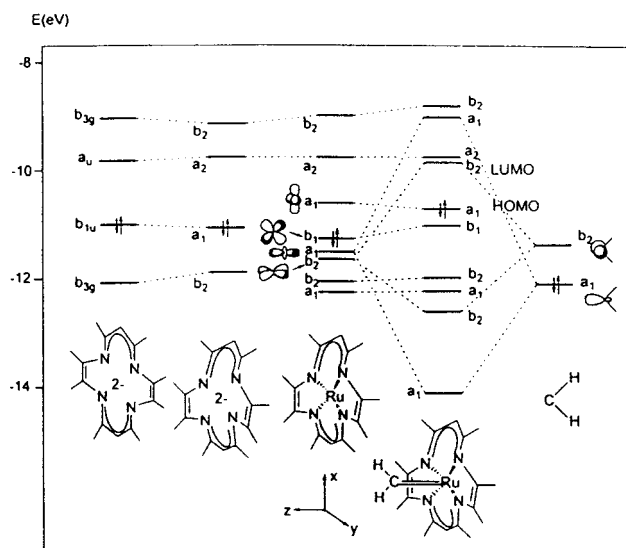
Figure 5. Building of the molecular orbitals of [Ru(tmtaa)] and orbital interaction diagram for [Ru(tmtaa)(CH$_2$)].

PMe$_3$ (Scheme 9) once again suggests, however, a free-radical pathway. This may be the consequence of the presence of the COOMe substituent at the carbene carbon having a significant π-acceptor contribution.

Extended Hückel Analysis on the [Ru(tmtaa)] Complexes. Extended Hückel calculations[32,33] were performed to elucidate the nature of the bonding in some of the complexes considered and to understand the labilization of the Ru–carbene functionality by a trans incoming ligand.

The molecular orbitals of the [Ru(tmtaa)] fragment are built in a step-by-step approach. We first considered the planar (tmtaa)$^{2-}$ ligand of D_{2h} symmetry, which was then deformed so as to reproduce the geometry of the (tmtaa) skeleton in the final complex.[2f,34] The molecular orbitals for the planar (tmtaa)$^{2-}$ ligand are reported in the first column of Figure 5, while in the second one we illustrate the effect of the bending up of the two benzo groups (18.5°) and the bending down of the two allyl groups (28.0°). We finally added Ru in the middle of the (tmtaa) ring, and the resulting MO diagram is reported in the third column of Figure 5. Upon coordination, the d orbitals mix strongly with the ligand frontier orbitals so that no pure d orbitals can be assigned. However five MOs with large metal d characters can be identified. These are the three highest occupied orbitals a$_1$(d$_{z^2}$), b$_2$-(d$_{yz}$), b$_1$(d$_{xz}$) and the lowest unoccupied orbital a$_1$(d$_{x^2-y^2}$) lying in the N$_4$ ligand plane. The a$_2$(d$_{xy}$) pointing more closely toward the nitrogen atoms of tmtaa is pushed high in energy. The second and third LUMOs correspond closely to the two LUMOs of the (tmtaa)$^{2-}$ distorted ligand, a$_u$ and b$_{3g}$.

We then considered the bonding between the CRR$'$ unit and the central metal in the [Ru(tmtaa)CRR$'$)] carbene complexes, first using the simplest R = R$'$ = H case, which enables us to simplify the discussion and change the orientation of the carbene plane without introducing steric effects. On the extreme right of Figure 5 we show the frontier orbitals of CH$_2$, i.e., the σ-donor

(32) Hoffmann, R.; Lipscomb, W. N. *J. Chem. Phys.* **1962**, *36*, 2179.
(33) Hoffmann, R. *J. Chem. Phys.* **1963**, *39*, 1397.
(34) Tatsumi, K.; Hoffmann, R. *Inorg. Chem.* **1981**, *20*, 3771.

Table 5. Main Parameters Describing the Interaction between the [Ru(tmtaa)] Metal Fragment and the CRR$'$ Moiety (See Text)

parameter	R, R$'$			
	H, H	Ph, H	Ph, Ph	Ph, COOMe
ϵ(b$_2$)	−11.40	−10.79	−11.03	−11.52
P(b$_2$)	0.95	0.76	0.87	1.10
Δ[HOMO$-\pi$*(M$-$C)]	1.54	1.00	0.87	0.43
Q(Ru)	+0.72	+0.46	+0.36	+0.58
Q(carbene-C)	−0.26	−0.21	−0.13	−0.21
Q(meso-C)	−0.30	−0.30	−0.30	−0.30
Q(CRR$'$)	−0.29	−0.14	−0.03	−0.33

a$_1$(sp^2 hybrid) and the π-acceptor b$_2$(p$_y$). The interaction between the [Ru(tmtaa)] fragment and the CH$_2$ unit is illustrated by the molecular orbital diagram for the [Ru-(tmtaa)(CH$_2$)] complex in the fourth column of Figure 5. In the [Ru(tmtaa)CPh$_2$)] complex, the only one whose X-ray structure is available, the orientation of the carbene unit is such that the CPh$_2$ plane forms an angle of about 39° with the xz symmetry plane bisecting the diiminato rings. However, to keep the C_{2v} symmetry of the metal fragment and simplify the analysis of the results, we considered an orientation with the CH$_2$ plane lying in the xz symmetry plane. Figure 5 shows a strong interaction between the 1a$_1$(d$_{z^2}$) and the σ-donor 1a$_1$ of CH$_2$ and between the 1b$_2$(d$_{yz}$) and the π-acceptor b$_2$. In principle the π-acceptor orbital of CH$_2$ could interact with both the doubly occupied b$_2$(d$_{yz}$) and b$_1$(d$_{xz}$) metal orbitals, leading to different orientations of the carbene moiety with the CH$_2$ unit lying in the xz and yz planes, respectively. The latter orientation has been calculated as being ca. 0.3 eV more stable, probably due to the more favorable interaction of the carbene π-acceptor orbital with the higher-lying 1b$_1$(d$_{xz}$) donor orbital. The apparent disagreement with the experimental X-ray structure can be rationalized by noting that the electronically most favorable orientation of the carbene moiety along the yz plane would lead to strong steric repulsion between the two bent benzo groups and the carbene phenyl substituents. The observed orientation is therefore a compromise between electronic factors favoring the orientation of the CPh$_2$ in the yz plane and steric repulsion favoring the orientation of the carbene in the xz plane. A calculation performed on the real CPh$_2$ carbene confirmed that the orientation of the carbene plane in the yz plane would lead to a strong steric destabilization.

Extended Hückel calculations have been performed on all the synthesized [Ru(tmtaa)(CRR$'$)] complexes **6**−**8** with R = R$'$ = Ph; R = Ph, R$'$ = H; and R = Ph, R$'$ = COOMe, respectively. The molecular orbital diagrams for these complexes is quite similar to that in Figure 5 for the CH$_2$ carbene. However, the presence of different substituents on the carbene unit affects the energy of the π-acceptor orbital b$_2$(p$_y$), thus changing some details of the molecular orbital diagram. In Table 5 we report the main parameter describing the interaction between the metal fragment and the CRR$'$ group, notably (i) the energy of the CRR$'$ π-acceptor orbital; (ii) its population in the carbene complex; (iii) the energy gap between the HOMO (mainly a d$_{x^2-y^2}$ metal orbital in all cases) and the low-lying orbital of antibonding d$_{yz}$(Ru)$-$p$_y$(C) π(M$-$C) character; (iv) the atomic charge on ruthenium, carbene carbon, and diiminato meso-carbon atom; (v)
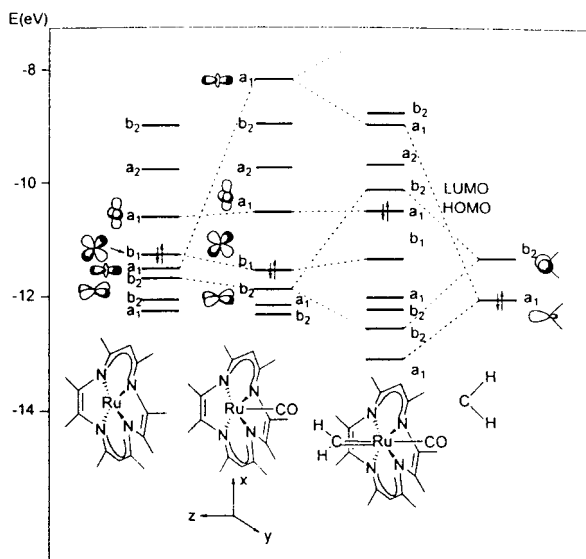
Figure 6. Orbital interaction diagram for [Ru(tmtaa)(CO)-(CH$_2$)] showing the effect of CO coordination.

the electron donation from the metal fragment to the CRR′ group.

For all these complexes, the interaction between the [Ru(tmtaa)] fragment and the CRR′ group is typical of most of the known metal carbene species.[35] In particular frontier orbital criteria suggest a Fisher carbene nature for this [Ru(tmtaa)(CRR′)] species rather than a Schrock alkylidene, in accordance with the accepted terminology. This is supported by (i) the low energy of the metal d$_\pi$ orbitals, lower than that of the π-acceptor b$_2$ orbitals (see Table 5); and (ii) the presence of a low-lying π^*-(M−C) LUMO of high carbon character (see Figure 5) which gives a significant electrophilic character to the carbene moiety, both effects being characteristic of Fisher carbene systems. However, the carbene unit shows a significant, although small, negative charge on the carbon atom ($-0.1/-0.3$) and a significant population on the π-acceptor b$_2$, which are more typical of Schrock alkylidenes. Therefore, **6−8** can be actually described as intermediate between Fisher carbene and Schrock alkylidene, without a definite electrophilic or nucleophilic character of the carbene carbon, in agreement with the observed poor reactivity toward both nucleophilic and electrophilic species. We did not observe any reactivity with either lithium alkyls or B(C$_6$F$_5$)$_3$. The small positive charge calculated on the ruthenium atom ($+0.3/+0.7$) and the small electron donation of the [Ru(tmtaa)] fragment to the CRR′ moiety upon carbene formation (0.03/0.33) (see Table 5) lend evidence to the attribution of a formal oxidation state of II and a d^6 configuration for ruthenium based on geometrical evidence (see above).

We then considered the effect of the coordination of a further ligand trans to the carbene unit. Figure 6 shows the effect of the CO coordination (a ligand with both σ-basic and π-acid properties) on the orbital levels of the [Ru(tmtaa)] fragment and its consequences on the interaction diagram between the resulting [Ru(tmtaa)-(CO)] fragment and the CH$_2$ unit. Figure 6 shows a

(35) Hoffmann, P. In *Transition Metal Carbene Complexes*; Dötz, K. H., Fischer, H., Hoffmann, P., Kreissl, F. R., Schubert, U., Weiss, K., Eds.; Verlag Chemie: Weinheim, 1983; p 113.

strong destabilization of the d$_{z^2}$ orbital (interacting with the carbon lone pair of CO) and a significant stabilization of the two d$_{xz}$, d$_{yz}$ orbitals (due to their interactions with the empty π^* orbitals of CO). Both effects lead to a higher energy mismatch between these metal orbitals and the interacting counterparts on the carbene unit and thus to a labilization of the metal−carbene bonding. Extended Hückel calculations have been performed on complexes **6−8** coordinated by a trans Py, CO, and PMe$_3$ ligand. We used the X-ray geometry of **6** (with plausible values for the geometry of the H or COOMe carbene substituent in **7** and **8**) including the ligand at a suitable distance from ruthenium with the free molecule geometry. No significant variation of the parameters describing metal−carbene interaction is observed upon coordination of a weak σ-donating ligand like pyridine and is in agreement with the observed stability of **6−8** in the presence of pyridine, leading only to the hexacoordinated carbene species **15−17**. A different situation is observed for a strong π-acid (CO) or a strong σ-donating (PMe$_3$) ligand, for which a significant variation of these parameters is observed (mainly a reduction of the population of the π-acceptor orbital of carbene and a decrease in the energy gap between the HOMO, essentially a d$_{x^2-y^2}$ orbital, and the LUMO, of antibonding d$_{yz}$ (Ru)−p$_y$(C) character), showing a weakening of the metal−carbene bond. Therefore a labilization of the Ru-carbene functionality upon CO or PMe$_3$ coordination is expected for **6−8** and actually observed for **7** and **8**.

For complex **7** this labilization probably leads to a detachment of a :CRR′ carbene, which then inserts into a C−C bond of the diiminato ring, leading to the seven-membered metallacycle. Such a carbene-mediated mechanism is supported by the presence in the mother liquor of the reaction of *cis*- and *trans*-stilbene between **7** and PMe$_3$. A different situation is found for **8** (R = Ph, R′ = COOMe), for which the low energy of the p$_\pi$ CRR′ unit leads to a small HOMO−LUMO gap, which is further reduced by trans coordination by CO and PMe$_3$ (less than 0.3 eV). Therefore, upon trans coordination, **8** is expected to generate a free radical at the carbene carbon attacking the meso-position of the tmtaa ligand, then rearranging to the bridging moiety in **11**.

To explain why the carbene labilization is not observed for **6**, although plausible on purely electronic grounds, we should mention that the calculations concern only the first step of the Ru−carbene labilization, i.e. the initial trans coordination of the incoming ligand, and use the geometry of the unperturbed carbenes with the metal displaced by 0.374 Å from the N$_4$ average plane toward the carbene carbon (see above). However, the real labilization process proceeds behind the simple coordination, passing probably through an inversion of the out-of-plane of ruthenium from the carbene toward the incoming ligand. This inversion is suggested for example by the X-ray structure of **3**,[24] which shows an out-of-plane of Ru toward the CO ligand. For complex **6**, probably, the steric crowding of the phenyl susbtituents with the benzo groups of the tmtaa macrocycle does not allow such an out-of-plane inversion toward the coordinated ligand, thus preventing carbene labilization.

Conclusions

The macrocycle illustrated by the dibenzotetramethyltetraaza[14]annulene seems to be particularly appropri-

ate for supporting the ruthenium−carbene functionality. The preorganized quasi-planar N_4 chemical environment favors study of the reciprocal influence of the two coordination sites trans to each other and, in particular, facilitates investigation into which kind of ligand (i.e. CO, PMe_3, etc.) can induce the trans-labilization of the carbene functionality and by which mechanism, namely, free radical or carbene. The ligand-induced migration of the carbene to the macrocyclic ligand has important precedents in iron porphyrins of biological relevance. The theoretical approach has been used to explain the ligand-induced labilization of the carbene functionality.

Supporting Information Available: Tables giving crystal data and structure refinement, atomic coordinates, bond lengths and angles, anisotropic displacement parameters, and hydrogen coordinates for **5**, **6**, **11**, and **12** (17 pages). Ordering information is given on any current masthead page.

OM980898P